pp 872–887. © Royal Aeronautical Society 2020
doi:10.1017/aer.2019.158

Additive metal solutions to aircraft skin corrosion

N. Matthews
neil.matthews@ruag.com
RUAG Australia
836 Mountain Highway
Bayswater, Victoria, 3153
Australia

R. Jones and D. Peng
Centre of Expertise for Structural Mechanics
Department of Mechanical and Aerospace Engineering
Monash University
Clayton, Victoria, 3800
Australia

N. Phan and T. Nguyen
Structures Division
Naval Air Systems Command
Patuxent River
MD, 20670
USA

ABSTRACT

This paper focuses on the problem of skin corrosion on the upper wing surfaces of rib-stiffened aircraft. For maritime and military transport aircraft this often results in multiple co-located repairs. The common approach to corrosion damage in operational aircraft is to blend out the corrosion and rivet a mechanical doubler over the region. In particular this paper describes the results of a combined numerical and experimental investigation into the ability of the additive metal technology, Supersonic Particle Deposition (SPD), to restore the load-carrying capacity of rib-stiffened wing planks with simulated skin corrosion. The experimental results reveal that unrepaired skin corrosion can result in failure by yielding. The experimental results also reveal that SPD repairs to skin corrosion can restore the stress field in the structure, and can ensure that the load-carrying capability of the repaired structure is above proof load.

Keywords: Aircraft skin corrosion; additive metal technology; buckling load; experimental stress analysis; load carrying capacity; Design Limit Load

Received 29 April 2019; revised 21 August 2019; accepted 26 November 2019.
A version of this paper was first presented at the 18th Australian International Aerospace Congress in February 2019.

1.0 INTRODUCTION

The Aloha accident[1] was one of the first incidents to highlight the potential problem of multiple interacting corrosion repairs on aircraft skins. This incident revealed the in presence of external-authorized patch repairs to address multi-site damage, catastrophic failure occurred when cracking ran from corrosion repair to corrosion repair, as seen in Fig. 1.

The problem of skin corrosion on upper wing surfaces, which is a focal point of this paper, is seen in many areas of the P3C (Orion) and often results in multiple co-located repairs (see Fig. 2). The common approach to corrosion damage in operational aircraft is to blend out the corrosion and rivet a mechanical doubler over the region (see Figs. 1 and 2). Unfortunately, if the aircraft is operated in an aggressive environment, corrosion can occur over a (relatively) broad area, and this can lead to a number of mechanical repairs that lie in relatively close proximity. This repair process involves drilling holes that act as stress concentrators in the base structure; unless the operational environment changes, these holes now provide additional sites at which corrosion can develop and with the potential of crack initiation and growth.

In this context it has been shown[2–6] that, the RUAG Australia's patented supersonic particle deposition (SPD) process, which uses aluminium alloy 7075 metal powder with particles sizes in the range of 30–50μm, has the potential to address a range of problems associated with aircraft structural integrity. Indeed[4,5], presented the results of a full-scale fatigue test on an F/A-18 centre barrel that had 12 SPD doublers applied to a range of features, which was subjected to a measured operational RAAF spectrum. These doublers were found to experience peak stresses of up to 250MPa without, at 18500 simulated flight hours (which is in excess of three design life times), any evidence of cracking or delamination[4,5]. As such this test when taken in conjunction with laboratory test results[4,5] highlight the fact that SPD can withstand representative flight load spectra with peak stresses greater than 200MPa[6].

RUAG Australia has led a 10-year program of research and development of SPD technology, and its technical efforts and outcomes have been instrumental to sustainment of the Australian Defence Force's aerospace capability. This program to-date has focused on the recovery of metal components and has been undertaken in close collaboration with the Australian Defence research establishment, academia and the Australian Defence airworthiness authority. The SPD applications have been implemented for substrate geometry restoration, corrosion protection and wear resistance. RUAG Australia has focused released in excess of 50 certified repaired products that have achieved in excess of 10,000 accrued flight hours on three aircraft types. Applications include numerous powder types on numerous substrate materials[7,8].

The potential of SPD to repair skin corrosion on tension dominated surfaces was highlighted in Refs. (3, 5 and 9). The capability of SPD to restore the load-carrying capacity of rib-stiffened wing planks under compression loading with stress corrosion cracking in the risers has been established in Refs. (5 and 6). The extensive 3D finite element analysis presented in Ref. (6) revealed the potential for SPD to restore the load bearing capacity of rib-stiffened wing structures where the upper wing skin was badly corroded and under compression loading. This paper presents the experimental verification of the 3D analysis[6] utilising sections of retired P3C (Orion) upper wing planks with geometries representative of corrosion damage. It is shown that skin corrosion can change the failure mode from global buckling to a local failure due to exceeding the load carrying capacity of the remaining ligament. It is also shown that SPD can restore the load carrying capacity of the structure.

Lock-in thermography was used for stress analysis of specimens. This technology enables conducting stress analysis and estimation of fatigue limits in a non-destructive and

https://doi.org/10.1017/aer.2019.158 Published online by Cambridge University Press

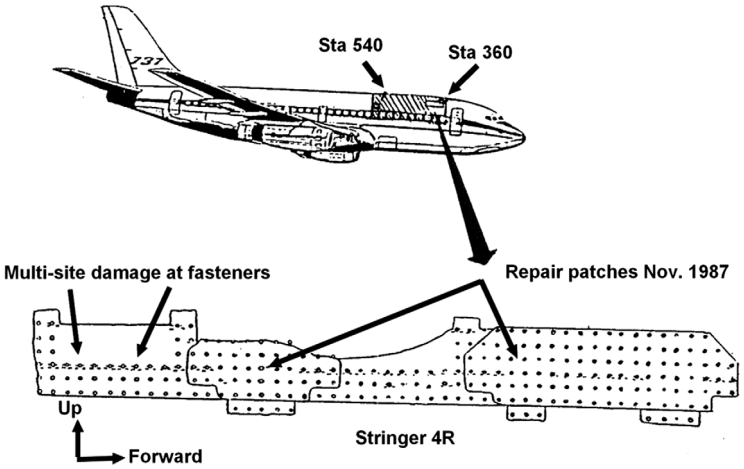

Figure 1. The linking from multiple repairs in the Aloha, from[1].

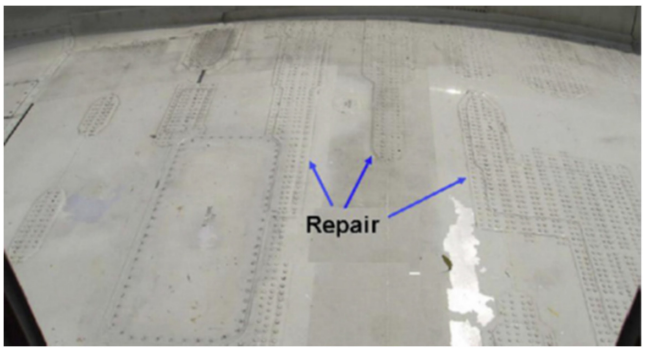

Figure 2. Multiple corrosion repairs on a P3C aircraft wing.

non-contact method within a shorter period, and thus users can obtain stress maps immediately after the test[10].

2.0 THE TEST PROGRAM

Whereas the finite element analysis study presented in Ref. (6) focused on assessing the effect of simulated corrosion on the stress distribution in un-corroded and (simulated) corroded P3C wing skin specimens, this experimental test program focused on assessing the capability of SPD repairs to restore the load-carrying capacity of specimens with simulated corrosion. Tests were performed on pristine, simulated corrosion and SPD repaired specimens. To this end five (5) P3C wing plank specimens were tested, viz:

- One pristine specimen (Specimen 1) in the "undamaged" configuration.
- One pristine specimen (Specimen 6) in the "undamaged" configuration. This specimen was used to further establish the stress distribution in a pristine specimen. It was chosen since its dimensions were similar to that of Specimen 5, which contained

https://doi.org/10.1017/aer.2019.158 Published online by Cambridge University Press

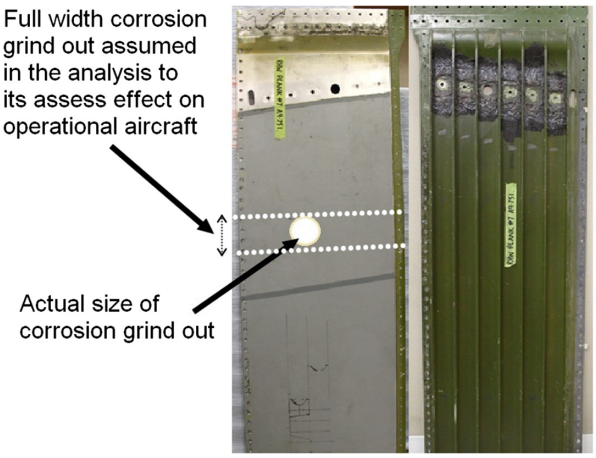

Figure 3. Exterior and Interior Views of RHW#07 Upper Wing Panel (P/N 938807-102).

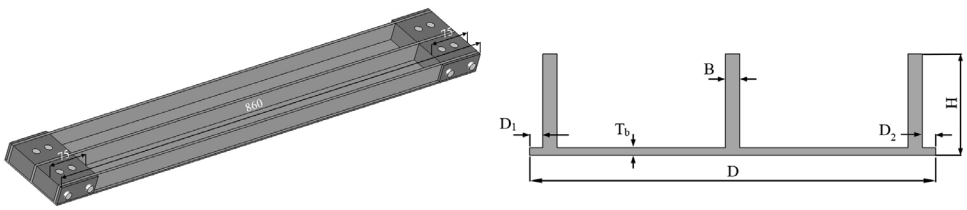

Figure 4. Pristine specimen.

simulated corrosion and was repaired using SPD. This test thereby enabled a direct comparison with Specimen 5.

- Two specimens (Specimens 2 and 4), which both had (unrepaired) simulated corrosion.
- Two specimens (Specimens 3 and 5) with SPD repairs to the simulated corrosion.

After discussions with Australian P3 user group, observed corrosion is generally circular. However, because of the difficulty in analysing this geometry a full-width corrosion grindout is normally assumed when the assessment of the impact of corrosion is conducted (refer to Fig. 3). Consequently, to more closely represent actual corrosion profiles, the effect of circular corrosion that lies between two risers has been evaluated.

Specimens were cut from three different P3C wing panels. The nominal geometry of the pristine specimen is as shown in Fig. 4. The nominal geometry of the simulated corrosion specimen is shown in Fig. 5. SPD of aluminium alloy 7075 metal powder with particles sizes in the range of 30–50μm was used to restore the panel geometry. Aluminium alloy 7075 metal powder was selected for its post-deposited mechanical properties and its similarity to the substrate material to avoid dissimilar metal potential corrosion. The nominal geometry of the SPD repair is shown in Fig. 6. The dimensions of the test specimens are provided in Table 1.

Tests to failure were performed on pristine Specimen 1, on Specimens 2 and 4 that contained simulated corrosion but were not repaired and on the SPD repaired panels Specimens 3

https://doi.org/10.1017/aer.2019.158 Published online by Cambridge University Press

Table 1
Specimen dimensions, the notation used is as per Figs. 4–6

Dimensions	Specimen Number					
	1 (mm)	2 (mm)	3 (mm)	4 (mm)	5 (mm)	6 (mm)
B	4.27	4.37	3.97	4.07	3.95	3.98
H	32.80	32.90	30.70	30.90	30.60	31.20
D	122.40	122.00	113.00	114.50	113.90	113.70
D_1	4.00	3.00	1.50	2.00	2.00	1.50
D_2	4.50	4.50	2.30	2.00	0.50	1.00
T_B	2.26	2.72	2.25	2.32	2.22	2.46
T_c	–	0.95	0.93	1.38	1.05	–
T_s	–	–	2.73	–	2.42	–

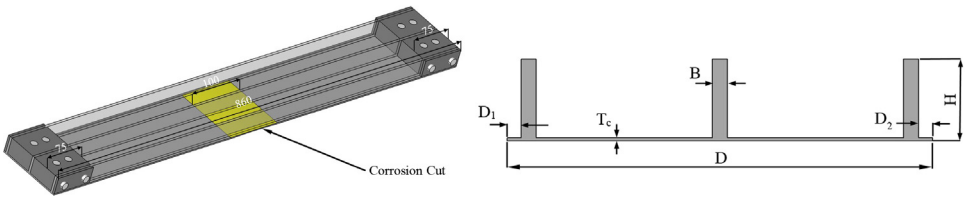

Figure 5. Specimen with simulated corrosion.

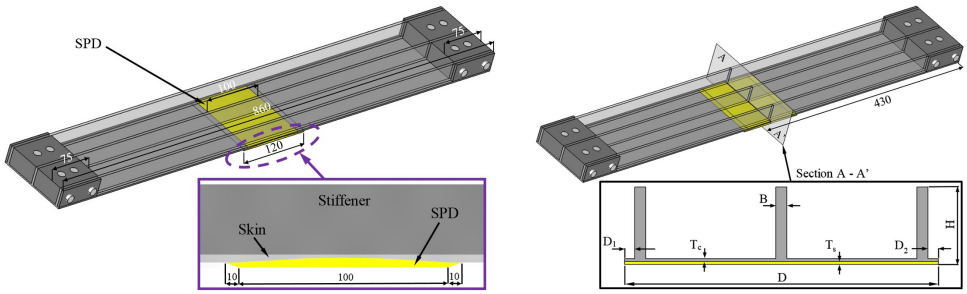

Figure 6. Specimen with SPD repair to the simulated corrosion.

and 5. The strain gauges were installed on these specimens. The locations of the strain gauges on these specimens are shown in Figs. 7–11.

The stress (in the skin) versus load curves associated with the pristine specimen, i.e. Specimen 1, is shown in Fig. 12. Here we see that the response was essentially linear (elastic) with load so that the specimen saw elastic buckling. We also see that Gauge 3, which was located in the centre of the specimen, has essentially the same reading as gauges 1 and 2, which are located closer to the grips. The elastic buckling associated with Specimen 1 is confirmed in Fig. 13, which shows the specimen after it has been removed from the test rig. Here we see that the specimen has essentially returned to its original shape.

https://doi.org/10.1017/aer.2019.158 Published online by Cambridge University Press

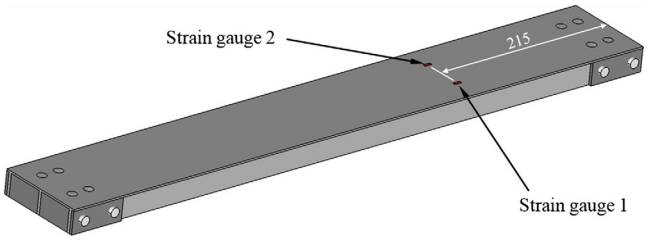

Figure 7. Location of the strain gauges on the front surface of the baseline (un-corroded) specimens.

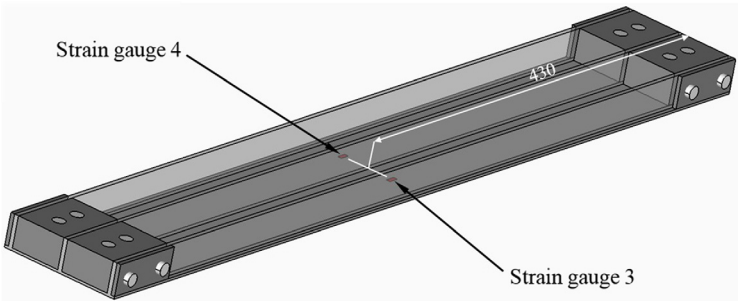

Figure 8. Location of the strain gauges on the back surface of the baseline (un-corroded) specimens.

The strain and stress versus load curves associated with simulated corrosion Specimens 2 and 4 are presented in Figs. 14–17, respectively. Figures 14 and 16 reveal that the simulated corrosion resulted in large out of plane displacements and that, as a result, large (post-yield) strains were seen in the skin at the location of the simulated corrosion. In contrast the regions remote from the simulated corrosion remained elastic. Figures 15 and 17 reveal that under loading up to approximately −65.4kN and −67.8kN the skin is behaving linearly for Specimens 2 and 4, respectively. Once these loads have been reached, the skin in the vicinity of the simulated corrosion experiences large elastic deformations with yielding commencing at approximately −127.7kN and −116.6kN for Specimen 2 and Specimen 4, respectively. (Here it should be noted that MILHDBK 5 lists the yield stress of the 7075-T6 wing skin as approximately 480MPa.) However, since in accordance with JSSG2006[3] yielding is not allowed at 115% design limit load, this means that the maximum load that this panel could take and still meet the requirements of JSSG2006 that there is no yielding in the wing skin is approximately 101kN. This corresponds to a remote stress, as determined from the remote strain gauges, of approximately 177MPa.

In Fig. 18 the testing to failure of Specimen 2 with the simulated corrosion clearly showed the effect of the localised buckling and the associated plastic yielding. The failure mode confirms the computational and experimental results presented in Ref. (5), namely that failure can be a local failure rather than the global buckling failure that is associated with a pristine specimen.

The strain and stress versus load curves associated with SPD Specimens 3 and 5 are presented in Figs. 19–22, respectively. Figures 19 and 21 reveal that up to approximately

https://doi.org/10.1017/aer.2019.158 Published online by Cambridge University Press

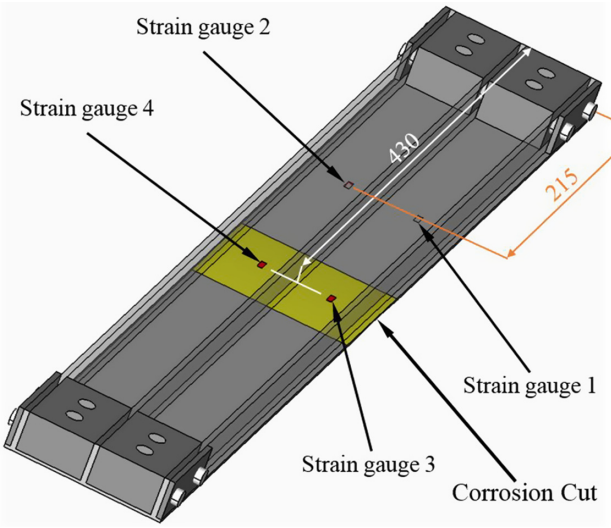

Figure 9. Location of the strain gauges on the back surface of the simulated corrosion specimens.

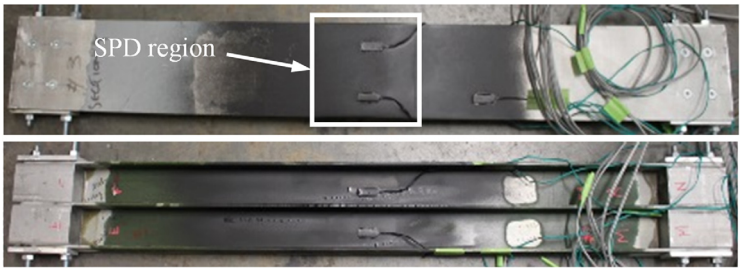

Figure 10. Specimen 3 (with SPD repair).

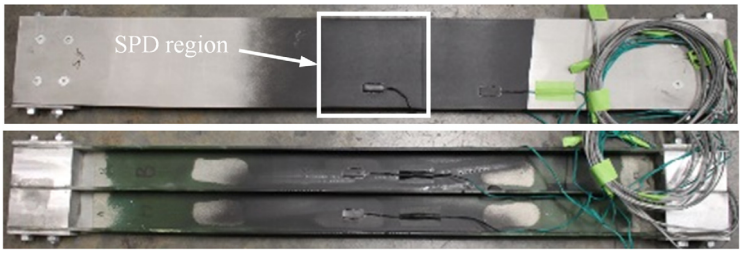

Figure 11. Specimen 5 (with SPD repair).

−160kN, the skin is behaving linearly. After an applied load of approximately −160.0kN, the specimens began to experience a nonlinear behaviour (see Figs. 20 and 22). Photographs of the failed Specimens 3 and 5 are shown in Figs. 23 and 24, respectively. In the case of Specimen 5, the SPD restored the buckling load to that of a pristine specimen; post-buckling

https://doi.org/10.1017/aer.2019.158 Published online by Cambridge University Press

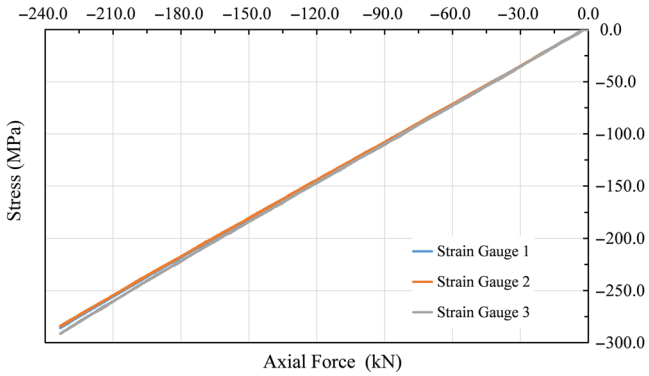

Figure 12. Comparison of the stress versus force, up to the onset of buckling, for the pristine specimen, i.e. Specimen 1.

Figure 13. Specimen 1 after testing.

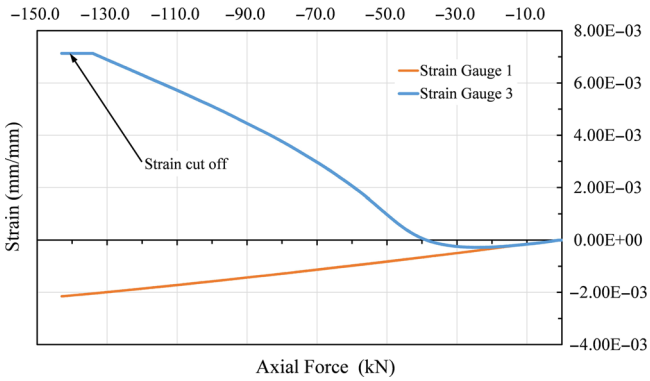

Figure 14. The strain versus force curves for simulated corrosion Specimen 2.

resulted in both cracking and partial disbonding of the SPD. In both cases the remote stresses in the skin were measured as being above 300MPa (see Figs. 20 and 22). Given that at Design Limit Load[1] the peak stresses seen in the P3C wing skin are less than approximately 180MPa, this means that *the SPD repairs withstood proof load without failure.*

[1]For military aircraft the certification requirement as delineated in JSSG2006[(4)] is that the airframe must be able to withstand Proof Load (=1.5 × Design Limit Load) without failure.

https://doi.org/10.1017/aer.2019.158 Published online by Cambridge University Press

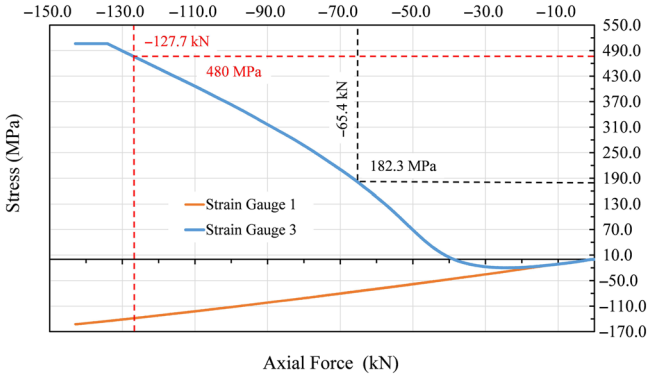

Figure 15. The stress versus force curves for simulated corrosion Specimen 2.

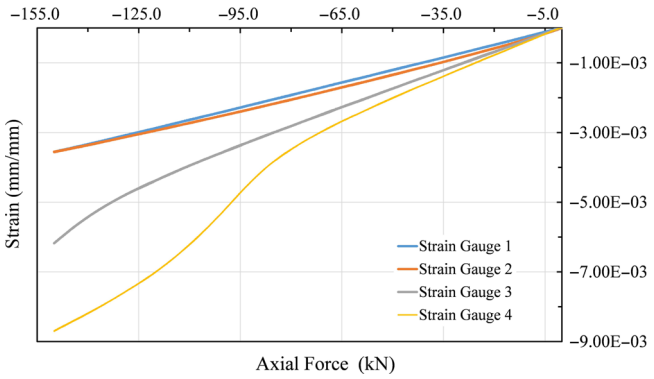

Figure 16. The strain versus force curves for simulated corrosion Specimen 4.

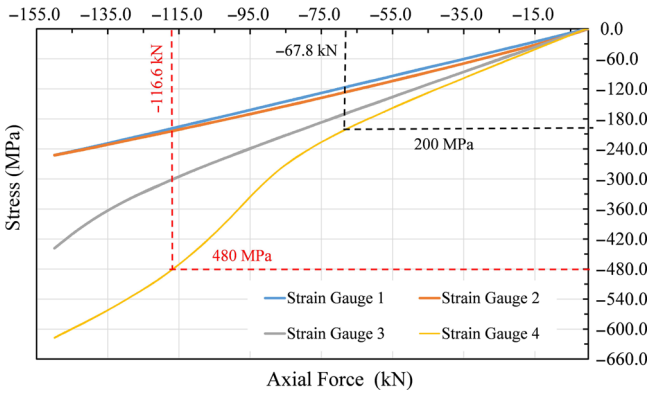

Figure 17. The stress versus force curves for simulated corrosion Specimen 4.

https://doi.org/10.1017/aer.2019.158 Published online by Cambridge University Press

Figure 18. Simulated corrosion Specimen 2 after testing showing the effect of the localised buckling.

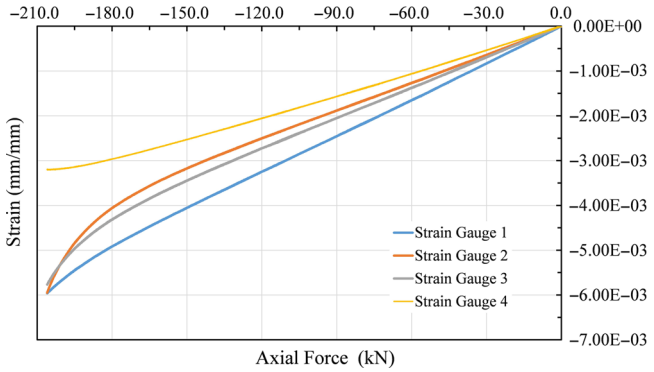

Figure 19. The strain versus force curves for Specimen 3 (with SPD repair).

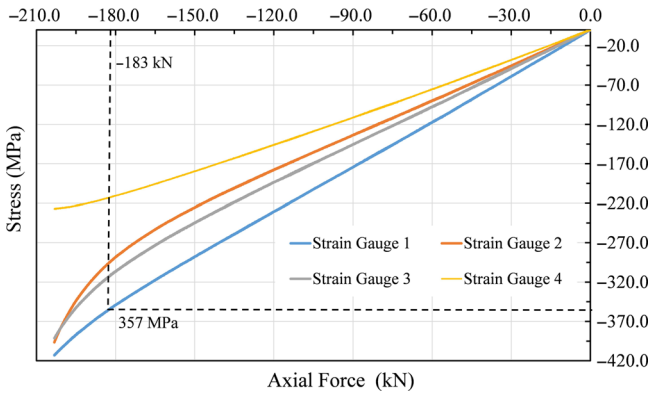

Figure 20. The stress versus force curves for Specimen 3 (with SPD repair).

The resultant load deflection curves and a comparison of the buckling loads associated with the pristine specimen, specimens with simulated corrosion damage and specimens repaired using SPD is presented in Fig. 25 and in Table 2. Here it should be noted that the differences in the initial slopes of the load deflection curves is due to the differences in the specimen

https://doi.org/10.1017/aer.2019.158 Published online by Cambridge University Press

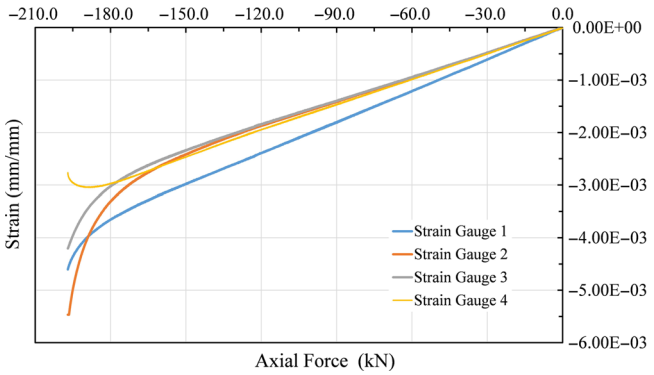

Figure 21. The strain versus force curves for Specimen 5 (with SPD repair).

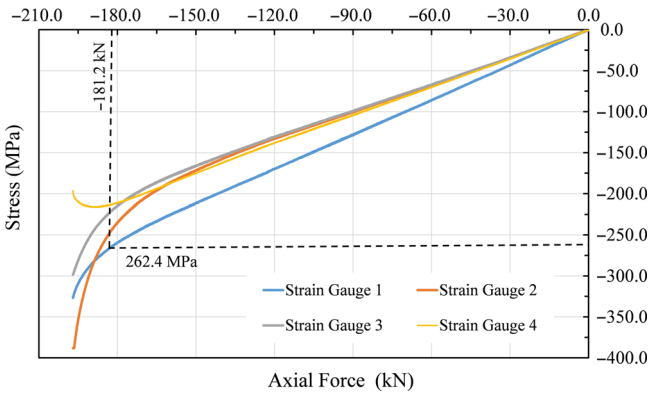

Figure 22. The stress versus force curves for Specimen 5 (with SPD repair).

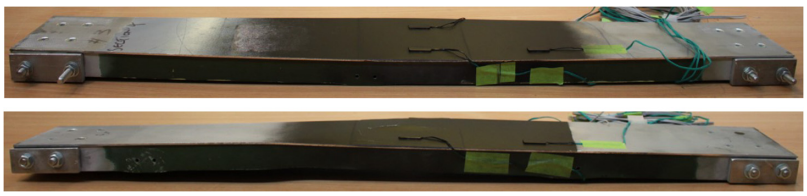

Figure 23. Specimen 5 after testing.

geometries. For example, since the thickness of the ribs in Specimen 1 is significantly greater than that of the ribs in Specimens 3 and 5 (the SPD repaired specimens), the slopes of the load-deflection curves differ. This was confirmed by static tests on specimens prior to the machining of the simulated corrosion.

https://doi.org/10.1017/aer.2019.158 Published online by Cambridge University Press

Figure 24. Specimen 5 after testing.

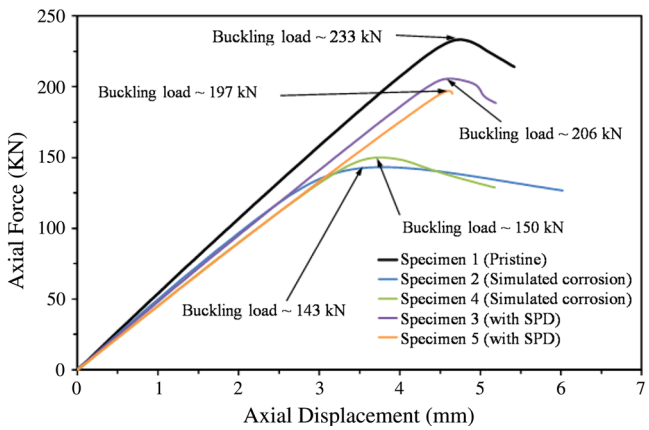

Figure 25. Load deflection and buckling loads associated with each specimen.

Furthermore, as shown in Table 2, the computed and measured buckling loads agreed to within 4%.

3.0 VALIDATION OF STRESS DISTRIBUTION ANALYSIS USING THERMOGRAPHY

Lock-in thermography was used for stress analysis of specimens, see Fig. 26.

This technology enables conducting stress analysis and estimation of fatigue limits in a nondestructive and non-contact method within a shorter period, and thus users can obtain stress maps immediately after the test[10].

Prior to testing the SPD repaired specimens (Specimen 3 and 5), strain gauge measurements and infra-red thermography stress measurements were performed in the unrepaired configuration along with pristine Specimen 6 (see Fig. 27). The tests were repeated with SPD repairs being incorporated in Specimens 3 and 5 (see Fig. 28). Two test programs were performed:

https://doi.org/10.1017/aer.2019.158 Published online by Cambridge University Press

Table 2
Buckling loads associated with Specimens 1–5

Specimen	Buckling load (kN)	Comment	Computed buckling load for the test geometry in kN. The percentage difference from the measured buckling load is in brackets
1 (pristine specimen)	233	Elastic buckling. On unloading the specimen returned to its original shape.	243 (4%)
2 (simulated corrosion)	143	Extensive plastic yielding. On unloading the specimen was extensively deformed.	143 (1%)
3 (SPD repair to simulated corrosion)	206	Elastic buckling. On unloading the specimen returned to its original shape. *The remote failure stain exceeded the Proof Load strains for the wing.*	For a specimen with the same geometry but with no simulated corrosion and no SPD the computed buckling load was 218kN. Thus allowing for errors the SPD repair essentially restored the buckling load to that of a pristine panel.
4 (simulated corrosion)	150	Plastic yielding. On unloading the specimen permanently deformed.	159 (6%)
5 (SPD repair)	197	The SPD restored the buckling load. *The remote failure stain exceeded the Proof Load strains for the wing.*	For a pristine specimen with the same geometry, i.e. with no simulated corrosion and no SPD, the computed buckling load was 206kN. Thus allowing for errors the SPD essentially restored the buckling load to that of a pristine panel.

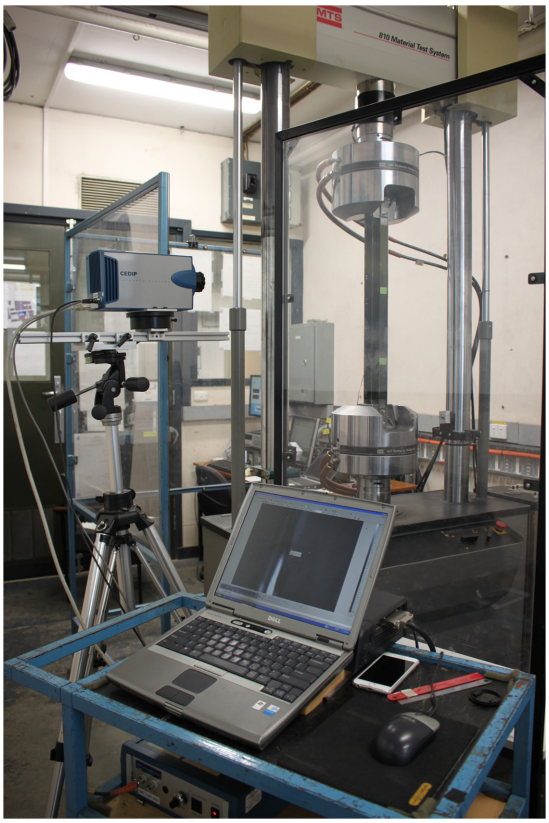

Figure 26. Specimen installed in the servo-hydraulic test machine and the infra-red camera.

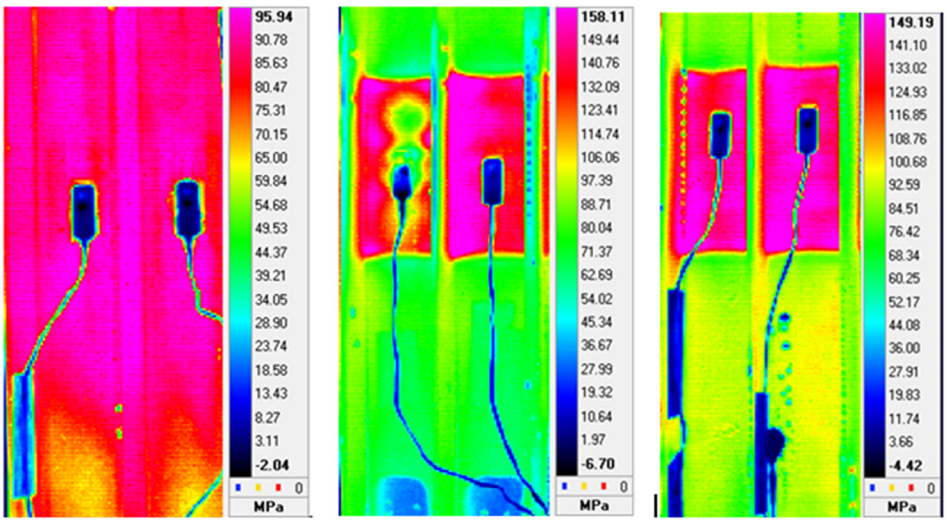

Figure 27. Thermography stress distribution – Specimens 6 (pristine), Specimen 3 (unrepaired) and Specimen 5 (unrepaired).

https://doi.org/10.1017/aer.2019.158 Published online by Cambridge University Press

Table 3
Measured stresses at −50kN using strain gauges

Compression (−50kN)	Location 1	2	3	4
	(MPa)			
Specimen 3 (SPD)	−92.7	−71.5	−77.2	−60.8
Specimen 5 (SPD)	−99.8	−80.6	−79.6	−82.9
Specimen 6 (Pristine)	−99.1	−96.9	−99.4	−99.1

Table 4
Stress range measured during infra-red thermography test

Cyclic test with loads ranging from (−5 to −55kN)	Location 1	2	3	4
	(MPa)			
Specimen 3 (SPD)	−92.8	−71.7	−78.0	−61.2
Specimen 5 (SPD)	−99.4	−80	−78.7	−82
Specimen 6 (Pristine)	−99.6	−95.7	−98.7	−99.2

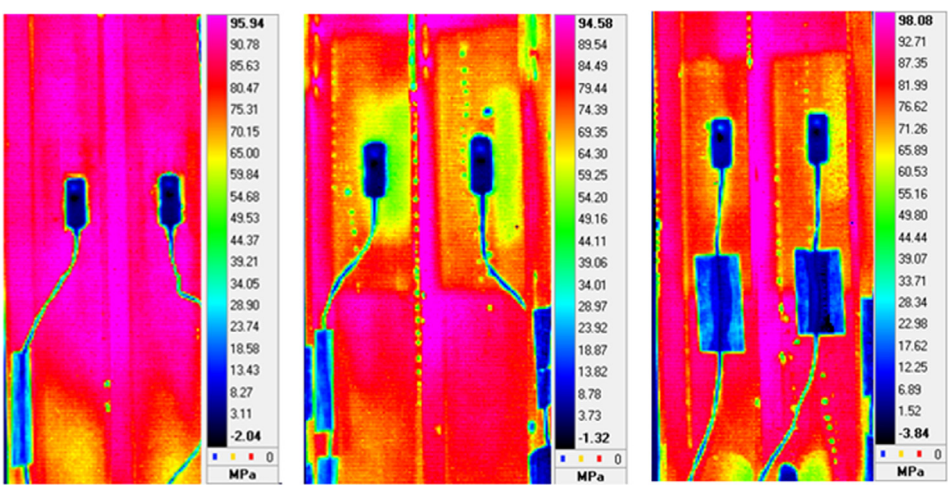

Figure 28. Thermography stress distribution – Specimens 6 (pristine), Specimen 3 (SPD repaired) and Specimen 5 (SPF repaired).

- A static compression test with the loads varying from 0 to −50kN.
- A cyclic load test with the loads varying from 5 to 55kN at a frequency of 4Hz.

As shown in Tables 3 and 4 excellent agreement was obtained.

https://doi.org/10.1017/aer.2019.158 Published online by Cambridge University Press

4.0 CONCLUSION

The present paper has confirmed prior analytical studies in that it has shown that SPD can be used to repair skin corrosion in rib-stiffened wing skins. Whilst the specific focus is on wing planks with geometries representative of P3C (Orion) upper wing planks, the results should be equally applicable to other aircraft which have a similar wing structure (e.g. C130 Transport aircraft). It is found that skin corrosion can change the failure mode from global buckling to a local failure due to exceeding the load carrying capacity of the remaining ligament. It is also found that SPD can restore the load carrying capacity of the structure to a level in excess of that associated with proof load.

REFERENCES

1. HENDRICKS, W.R. The Aloha-Airlines accident – a new era for aging aircraft. In *Structural Integrity of Aging Airplanes*, Atluri S.N., Sampath S.G. and Tong P., (Eds), Springer-Verlag, 1991, Berlin, Heildelberg, pp 153–165.
2. JONES R., MATTHEWS N., RODOPOULOS C.A., CAIRNS K. and PITT S. On the use of supersonic particle deposition to restore the structural integrity of damaged aircraft structures, *Int J Fatigue*, 2011, **33**, (9), pp 1257–1267.
3. JONES R., MATTHEWS N., GREEN R. and PENG D. On the potential of supersonic particle deposition to repair simulated corrosion damage, *Eng Fract Mech*, 2015, **137**, pp 26–33.
4. JONES R., MOLENT L., BARTER S., MATTHEWS N. and TAMBOLI D. Supersonic particle deposition as a means for enhancing the structural integrity of aircraft structures, *Int J Fatigue*, 2014, **68**, pp 260–268.
5. JONES R., MATTHEWS N., PENG D., PHAN N. and NGUYEN T. Applications of SPD to enhance the structural integrity of corroded airframes. In *Aircraft Sustainment and Repair*, Jones R.N., Matthews A.A.B. and Champagne V., Jr., (Eds) Elsevier Butterworth-Heinemann Press, 2018, Oxford, UK, Chapter 16, pp 863–906, ISBN 9780081005408.
6. JONES R., PENG D., MATTHEWS N. and ORCHOWSKI N. A study into the ability of SPD to restore the buckling strength and modes of rib stiffened panels with simulated stress corrosion cracks, *Int J Struct Integr*, 2017, **8**, (1), pp 63–78.
7. CHAMPAGNE V., Jr., MATTHEWS N. and CHAMPAGNE V., III. Introduction to supersonic particle deposition. In *Aircraft Sustainment and Repair*, Jones R., Matthews N., Baker A.A. and Champagne V., Jr., (Eds), Elsevier Butterworth-Heinemann Press, 2018, Oxford, UK, Chapter 14, pp 799–840, ISBN 9780081005408.
8. MATTHEWS N. Additive metal technologies for aerospace sustainment management. In *Aircraft Sustainment and Repair*, Jones R., Matthews N., Baker A.A. and Champagne V., Jr., (Eds), Elsevier Butterworth-Heinemann Press, 2018, Oxford, UK, Chapter 15, pp 845–861, ISBN 9780081005408.
9. MATTHEWS N., MOLENT L., BARTER S. and JONES R. Application of SPD to enhance the structural integrity of fuselage skins and centre barrels metal technologies for aerospace sustainment management. In *Aircraft Sustainment and Repair*, Jones R., Matthews N., Baker A.A. and Champagne V., Jr., (Eds), Elsevier Butterworth-Heinemann Press, 2018, Oxford, UK, Chapter 17, pp 907–929, ISBN 9780081005408.
10. JONES R., KRISHNAPILLAI M., CAIRNS K. and MATHEWS N. Application of infrared thermography to study crack growth and fatigue life extension procedures, *Fatigue Fract Eng Mater Struct*, 2010, **33**, (12), pp 871–884.

https://doi.org/10.1017/aer.2019.158 Published online by Cambridge University Press